

1 **Loss-of-function mutation in Omicron variants reduces spike protein expression and**  
2 **attenuates SARS-CoV-2 infection**

3 Michelle N. Vu<sup>1</sup>, Dorothea R. Morris<sup>1,2</sup>, R. Elias Alvarado<sup>1,3</sup>, Kumari G. Lokugamage<sup>1</sup>, Yiyang  
4 Zhou<sup>4</sup>, Leah K. Estes<sup>1</sup>, Alyssa M. McLeland<sup>1</sup>, Craig Schindewolf<sup>1</sup>, Jessica A. Plante<sup>1, 5, 6</sup>, Yani P.  
5 Ahearn<sup>1</sup>, Angelica L. Morgan<sup>7</sup>, William M. Meyers<sup>7</sup>, Jordan T. Murray<sup>1</sup>, Scott C. Weaver<sup>1, 5, 6, 8</sup>,  
6 David H. Walker<sup>7, 8</sup>, William K. Russell<sup>4</sup>, Andrew L. Routh<sup>4</sup>, Kenneth S. Plante<sup>1, 5, 6</sup>, Vineet  
7 Menachery<sup>1, 5, 6, 8\*</sup>

8 <sup>1</sup>Microbiology and Immunology, University of Texas Medical Branch, Galveston, TX, United  
9 States.

10 <sup>2</sup>Pediatrics, University of Texas Medical Branch, Galveston, TX, United States.

11 <sup>3</sup>Institute for Translational Sciences, University of Texas Medical Branch, Galveston, TX, United  
12 States.

13 <sup>4</sup>Biochemistry and Molecular Biology, University of Texas Medical Branch, Galveston, TX,  
14 United States.

15 <sup>5</sup>Institute for Human Infection and Immunity, University of Texas Medical Branch, Galveston, TX,  
16 United States.

17 <sup>6</sup>World Reference Center of Emerging Viruses and Arboviruses, University of Texas Medical  
18 Branch, Galveston, TX, United States.

19 <sup>7</sup>Pathology, University of Texas Medical Branch, Galveston, TX, United States.

20 <sup>8</sup>Center for Biodefense and Emerging Infectious Disease, University of Texas Medical Branch,  
21 Galveston, TX, United States.

22

23 \* Corresponding Author: Vineet D. Menachery, vimenach@utmb.edu

24 **Abstract**

25 SARS-CoV-2 Omicron variants emerged in 2022 with >30 novel amino acid mutations in the spike  
26 protein alone. While most studies focus on the impact of receptor binding domain changes,  
27 mutations in the C-terminal of S1 (CTS1), adjacent to the furin cleavage site, have largely been  
28 ignored. In this study, we examined three Omicron mutations in CTS1: H655Y, N679K, and  
29 P681H. Generating a SARS-CoV-2 triple mutant (YKH), we found that the mutant increased spike  
30 processing, consistent with prior reports for H655Y and P681H individually. Next, we generated  
31 a single N679K mutant, finding reduced viral replication *in vitro* and less disease *in vivo*.  
32 Mechanistically, the N679K mutant had reduced spike protein in purified virions compared to wild-  
33 type; spike protein decreases were further exacerbated in infected cell lysates. Importantly,  
34 exogenous spike expression also revealed that N679K reduced overall spike protein yield  
35 independent of infection. Together, the data show that N679K is a loss-of-function mutation  
36 reducing overall spike levels during omicron infection, which may have important implications for  
37 disease severity, immunity, and vaccine efficacy.

38

39 **One Sentence Summary**

40 Spike substitution N679K attenuates SARS-CoV-2 Omicron variants by decreasing spike protein  
41 and has potential implications for immunity and vaccine efficacy.

42 **Introduction**

43 Since its introduction, SARS-CoV-2 has continuously evolved giving rise to multiple  
44 Variants of Concern (VOCs) with diverse mutations in the spike protein (1). Present as a trimer  
45 on virions, spike is composed of S1 and S2 subunits, responsible for receptor binding and  
46 membrane fusion, respectively (2, 3). The S1 subunit contains the N-terminal domain (NTD),  
47 receptor binding domain (RBD), and the C-terminus of the S1 subunit (CTS1), which harbors a  
48 furin cleavage site (FCS) in SARS-CoV-2. Following receptor binding, the spike is cleaved at the  
49 S1/S2 site by host proteases to expose the fusion machinery for entry. With the diverse mutations  
50 in the spike protein, most Omicron studies have focused on the RBD and the impact on vaccine-  
51 or infection-induced immunity. However, mutations surrounding the FCS and S1/S2 cleavage site  
52 have been demonstrated to drive SARS-CoV-2 pathogenesis (4-9) and have been largely  
53 unstudied in the context of Omicron.

54 With this in mind, we set out to evaluate the role of Omicron CTS1 mutations on infection  
55 and pathogenesis. Omicron maintains three mutations adjacent to the FCS and S1/S2 cleavage  
56 site: H655Y, N679K, and P681H. Both H655Y and P681H have previously been observed in the  
57 Gamma and Alpha variants (10, 11); in contrast, N679K is unique to and maintained by all  
58 Omicron subvariants (12). To evaluate the role of these mutations, we used reverse genetics to  
59 generate SARS-CoV-2 mutants with all three CTS1 mutations (YKH) or N679K alone in the  
60 original WA1 backbone from early 2020. While YKH modestly increases viral replication and spike  
61 processing *in vitro*, N679K results in a loss-of-function mutation that attenuates viral replication *in*  
62 *vitro* and disease *in vivo* through reduced spike protein expression. Given the importance of spike  
63 protein for immunity, our finding may have major implications for vaccine efficacy and  
64 breakthrough infections.

65

66 **Results**

67 **H655Y, N679K, and P681H together increase viral replication and spike processing.**

68        While the majority of the > 30 spike mutations Omicron acquired are localized to the RBD,  
69        three are harbored in the CTS1 adjacent to the furin cleavage site – H655Y, N679K, and P681H  
70        (**Fig. 1A**). Both H655Y and P681H have been observed individually in Gamma and Alpha variants  
71        and are associated with increased spike processing. In contrast, N679K is a mutation unique to  
72        Omicron and is maintained in all subsequent Omicron subvariants despite involving a single  
73        nucleotide change (T/C to A/G) in the wobble codon position (12). Importantly, N679K is adjacent  
74        to an important O-linked glycosylation site at T678 (13, 14); our group has previously shown this  
75        glycosylation is important for SARS-CoV-2 infection and protease usage (8).

76        Several motifs within the CTS1 spike domain, including the furin cleavage site and the  
77        upstream QTQTN motif, are key to spike cleavage and host protease interactions, which drive  
78        SARS-CoV-2 infection and pathogenesis. All three Omicron mutations in the CTS1, H655Y,  
79        N679K, and P681H, are adjacent to or within these motifs and may impact their function (**Fig. 1A**  
80        and **1B**). To evaluate this, we generated a mutant SARS-CoV-2 harboring H655Y, N679K, and  
81        P681H in the original WA1 backbone (YKH) (**Fig. 1C**) (15, 16). Plaques produced by the YKH  
82        mutant were smaller compared to the parental WA1 (WT) (**Fig. 1D**). However, the YKH mutant  
83        did not attenuate stock titers nor replication kinetics in Vero E6 cells as compared to wild-type  
84        (WT) SARS-CoV-2 (**Fig. 1E and 1F**). Notably, while replication was slightly reduced at 24 hpi,  
85        end point titers for YKH were augmented at 48 hpi in Calu-3 2B4 cells compared to WT (**Fig. 1G**).  
86        The results suggest that the combination of the three mutations alters infection dynamics, which  
87        may offer some advantages to the Omicron variant in human respiratory cells (**Fig. 1G**). As H655Y  
88        and P681H have individually been shown to increase spike processing, we next evaluated spike  
89        processing on purified virions from YKH and WT infection. Similar to Delta and Omicron, YKH  
90        spike was more processed than WT (**Fig. 1H and 1I**). At 24 hpi, the S1/S2 cleavage ratio to full  
91        length spike ratio was ~2.4:1 for the YKH spike (55% S1/S2 product, 23% full-length); in contrast,

92 WT had roughly equivalent amounts of S1/S2 product and full length. Overall, the combination of  
93 H655Y, N679K, and P681H in the YKH mutant resulted in increased viral endpoint yields in human  
94 respiratory cells and contributed to Omicron's enhanced spike processing.

95 **N679K mutation attenuates SARS-CoV-2 infection.**

96 The increase in spike processing found in the YKH mutant is consistent with prior work  
97 examining H655Y and P681H mutations individually; however, the contribution of N679K had yet  
98 to be evaluated. Based on its location adjacent to a key O-linked glycosylation site, we  
99 hypothesized that N679K might impact SARS-CoV-2 infection (**Fig. 2A**). To evaluate potential  
100 changes, we generated a SARS-CoV-2 mutant with only N679K in the WA1 backbone (N679K)  
101 (**Fig. 2B**). Our initial characterization found that the N679K plaque sizes were distinctly smaller at  
102 days 2 and 3 post-infection (**Fig. 2C**), and stock titers were slightly lower than WT (**Fig. 2D**).  
103 These differences in plaque size and stock titers are consistent with other observations of most  
104 of the Omicron strains (17-20). Notably, unlike the minimal differences seen in YKH replication  
105 kinetics, the N679K mutant had attenuated replication in both Vero E6 and Calu-3 2B4 cells at 24  
106 hpi (**Fig. 2E and 2F**). Although N679K viral titer recovered by 48 hpi, the results suggest that  
107 N679K is a loss-of-function mutation in terms of replication in both cell lines.

108 We next evaluated N679K *in vivo* by infecting 3-to-4-week-old golden Syrian hamsters  
109 and monitored weight loss and disease over 7 days (**Fig. 2G**). Hamsters infected with N679K  
110 displayed significantly attenuated body weight loss compared to those infected with WT (**Fig. 2H**).  
111 Despite the stark attenuation seen in weight loss, N679K viral titers in the lungs were equivalent  
112 to WT at 2 dpi and 4 dpi (**Fig. 2I**). Similarly, N679K viral titers were comparable to WT at 2 dpi in  
113 nasal washes; however, the mutant virus resulted in reduced replication at 4 dpi (**Fig. 2J**). Taken  
114 together, our results indicate that N679K has a distinct loss-of-function phenotype *in vitro* and *in*  
115 *vivo*; given this result, we hypothesize that N679K loss-of-function is mitigated by the impact of  
116 the H655Y and P681H mutations.

117 **N679K mutation results in decreased spike protein expression.**

118        We next sought to determine the mechanism driving the loss-of-function observed with  
119    the N679K mutant. Given its location adjacent to the FCS, we first evaluated N679K effects on  
120    proteolytic spike processing. Virions were purified from WT, N679K or the Omicron variant BA.1  
121    (Omicron) and blotted for spike processing. Nearly identical to YKH, the N679K mutant had  
122    increased spike processing with a ~2.5:1 ratio of S1/S2 cleavage product to full-length spike  
123    compared to 1:1 ratio for WT at 24 hpi (**Fig. 3A and 3B**). However, we noted distinct differences  
124    in total spike protein with N679K and Omicron compared to WT, despite similar levels of  
125    nucleocapsid protein. Densitometry analysis revealed that the total spike to nucleocapsid (S/N)  
126    ratio of N679K and Omicron virions was reduced 21% and 36%, respectively, as compared to WT  
127    (**Fig. 3C**). Overall, our results indicate that the N679K mutant and Omicron variant incorporate  
128    less spike protein onto their virions.

129        We then sought to determine if changes in the virion spike were due to changes to total  
130    protein expression in the cell or incorporation into the particle. To examine spike protein  
131    expression, we measured total spike relative to nucleocapsid in infected Vero E6 cell lysates 24  
132    hpi (**Fig. 3D and 3E**). N679K resulted in a S/N ratio 66% less than WT, displaying an even further  
133    decrease in spike protein compared to the reduction in purified virions. Additionally, a similar  
134    decrease in S/N ratio was observed in Omicron, indicating that the phenotype is maintained in  
135    the context of all Omicron mutations (**Fig. 3D and 3E**). Together, the results indicate that the  
136    N679K mutation reduces the Omicron spike protein levels compared to WT.

137        Having established reduced spike protein in the context of N679K, we next wanted to  
138    determine if this reduction only occurs in the context of virus infection or is inherent to the protein.  
139    Therefore, we introduced the mutation into the Spike HexaPro plasmid to exogenously express  
140    spike protein to separate N679K driven changes from other aspects of viral infection (21). Vero  
141    E6 cells were transfected with the WT or N679K mutant spike HexaPro and harvested at 24 and  
142    48 hours post transfection (hpt). Similar to what was observed in viral infection, N679K spike was

143 reduced 43% at 24 hpt and 46% at 48 hpt (**Fig. 3F and 3G**). Overall, the results suggest that the  
144 reduction in Omicron spike is governed by N679K in a manner independent of viral infection.

145 **Discussion**

146 Most Omicron studies have focused on determining the impact that the RBD mutations  
147 have on immune escape, largely overlooking mutations in other spike domains like the CTS1.  
148 Harboring the FCS and S1/S2 cleavage site, the CTS1 has been demonstrated as a hotspot for  
149 both attenuating and augmenting mutations (4-9). Focusing on Omicron's three CTS1 mutations  
150 – H655Y, N679K, and P681H, we generated infectious clones with all three (YKH) or N679K alone  
151 in the SARS-CoV-2 WA1 background. The combination of YKH produced a modest increase in  
152 endpoint titers after infection of human respiratory cells, and augmented spike processing,  
153 consistent with prior studies that tested the effects of H655Y and P681H individually (10, 11).  
154 However, the N679K mutant reduced viral replication *in vitro* and weight loss *in vivo*. Mechanistic  
155 studies determined that both N679K and Omicron have reduced spike protein incorporated into  
156 their virions, less spike protein in infected cell lysates, and inferior production using exogenous  
157 spike protein expression systems compared to WT. Our results argue that reduced spike protein  
158 in the context the N679K mutation attenuates Omicron strains and may have implications for  
159 SARS-CoV-2 immunity by reducing spike antigen thus shifting immune recognition.

160 N679K is likely attenuated because of its decrease in spike protein production. Starting  
161 with ~30% less spike in its virions, one possibility was a change in spike incorporation. However,  
162 an even greater decrease (66%) in spike protein was present in infected Vero E6 cell lysates,  
163 indicated that overall spike protein levels were affected. To confirm that the reduction in spike  
164 was not a product of virus infection or host immune interactions, we exogenously expressed the  
165 spike protein to demonstrate that the N679K spike protein itself was less stable than the WT  
166 control. N679K, a single nucleotide and amino acid change, is unlikely to alter spike RNA  
167 expression and may instead act at the protein level. One possible mechanism is that the  
168 asparagine-to-lysine change introduces a ubiquitination site that could lead to spike degradation.

169 Another possible mechanism is that the N679K mutation itself may destabilize the protein  
170 structurally. Additionally, the N679K substitution adds another basic amino acid to the stretch  
171 including the FCS; the additional positively charged lysine extends the polybasic cleavage motif  
172 and may facilitate cleavage by additional host proteases (22). Overall, while the exact mechanism  
173 is unclear, the N679K mutation results in a less stable spike protein that impacts infection and  
174 pathogenesis of SARS-CoV-2.

175 Surprisingly, N679K is uniformly found in 100% of Omicron sequences in GSAID, despite  
176 being a single nucleotide change in the wobble position (12). Though attenuated *in vitro*, N679K  
177 does replicate to similar titers as WT in hamster lungs and at day 2 in nasal washes. These results  
178 suggest no deficits in transmission and may explain how N679K is maintained despite clear  
179 attenuation of SARS-CoV-2 infection. Notably, addition of H655Y and P681H in the YKH mutant  
180 rescues replication in Calu-3 cells, suggesting that other Omicron mutations may compensate for  
181 N679K. However, it is unclear if reverting N679K in the Omicron strains would result in a gain-of-  
182 function in terms of *in vitro* replication or *in vivo* pathogenesis. While N679K in SARS-CoV-2 WA1  
183 produces a clear loss-of-function, the constellation of spike mutations and epistatic interactions  
184 may mitigate the deficit in Omicron strains. Importantly, the complete conservation of N679K in  
185 Omicron also implies some fitness advantage; this may be in transmission, replication in certain  
186 cells/tissues, or evasion of host immune responses (23-28). While more studies are required to  
187 decipher why it is maintained, N679K is clearly a mutation that impacts overall spike protein  
188 expression.

189 In addition to impacting primary infection, the reduction in spike protein may have  
190 important implications for SARS-CoV-2 resistance to human immunity. Compared to WT, the  
191 N679K mutant produces less spike protein upon infection and can potentially skew the ratio of  
192 antibodies targeting spike and nucleocapsid. Prior work with SARS-CoV had shown that an  
193 altered spike/nucleocapsid antibody ratio contributed to vaccine failure in aged mice (29).  
194 Therefore, infection with Omicron could increase N targeting antibodies at the expense of spike

195 antibodies. The result would be less protective neutralizing antibody, which may facilitate more  
196 breakthrough infections. Furthermore, SARS-CoV-2 vaccines based on the Omicron spike may  
197 produce less spike protein due to N679K mutation. In the context of the mRNA bivalent vaccines,  
198 the N679K mutation may alter the 1:1 ratio of WT to Omicron spike protein; N679K may bias  
199 immune responses towards WT spike protein instead of equally between both spike proteins. In  
200 addition, the total amount of spike protein produced may be less than previous vaccines  
201 formulations, thus diminishing the overall antibody response. These factors potentially contribute  
202 to the less than expected increase in immunity against Omicron despite the new bivalent vaccine  
203 formulations. Moving forward, reverting K679 back to N679 in vaccine may improve spike protein  
204 yields and subsequently improve vaccine response to the Omicron variants.

205 Together, our results demonstrate that Omicron N679K is a loss-of-function mutation  
206 consistently maintained in subvariants. Mechanistically, the N679K mutation attenuates the virus  
207 *in vitro* and *in vivo* by increasing spike degradation. While the N679K mutation is attenuating in  
208 isolation, other Omicron mutations like H655Y and P681H may compensate for the N679K loss  
209 of function by amplifying spike processing and infection. However, the decreased spike protein  
210 expression by N679K may have implications for immunity induced by infection and vaccines.  
211 Overall, the interplay between the Omicron CTS1 mutations has a significant impact on SARS-  
212 CoV-2 infection and require additional studies for clarification.

213 **References**

- 214 1. E. Callaway, Heavily mutated Omicron variant puts scientists on alert. *Nature* **600**, 21 (2021).
- 215 2. S. Belouzard, J. K. Millet, B. N. Licitra, G. R. Whittaker, Mechanisms of Coronavirus Cell Entry  
216 Mediated by the Viral Spike Protein. *Viruses* **4**, 1011-1033 (2012).
- 217 3. M. N. Vu, V. D. Menachery, Binding and entering: COVID finds a new home. *PLOS Pathogens* **17**,  
218 e1009857 (2021).
- 219 4. B. Coutard *et al.*, The spike glycoprotein of the new coronavirus 2019-nCoV contains a furin-like  
220 cleavage site absent in CoV of the same clade. *Antiviral Research* **176**, 104742 (2020).
- 221 5. B. A. Johnson *et al.*, Loss of furin cleavage site attenuates SARS-CoV-2 pathogenesis. *Nature*,  
222 (2021).
- 223 6. Y. Liu *et al.*, Delta spike P681R mutation enhances SARS-CoV-2 fitness over Alpha variant. *bioRxiv*,  
224 2021.2008.2012.456173 (2021).
- 225 7. T. P. Peacock *et al.*, The furin cleavage site in the SARS-CoV-2 spike protein is required for  
226 transmission in ferrets. *Nat Microbiol* **6**, 899-909 (2021).
- 227 8. M. N. Vu *et al.*, QTQTN motif upstream of the furin-cleavage site plays a key role in SARS-CoV-2  
228 infection and pathogenesis. *Proceedings of the National Academy of Sciences* **119**, e2205690119  
229 (2022).
- 230 9. S.-Y. Lau *et al.*, Attenuated SARS-CoV-2 variants with deletions at the S1/S2 junction. *Emerging  
231 Microbes & Infections* **9**, 837-842 (2020).
- 232 10. A. Escalera *et al.*, Mutations in SARS-CoV-2 variants of concern link to increased spike cleavage  
233 and virus transmission. *Cell Host & Microbe* **30**, 373-387.e377 (2022).
- 234 11. Y. Liu *et al.*, Delta spike P681R mutation enhances SARS-CoV-2 fitness over Alpha variant. *Cell  
235 Reports* **39**, (2022).
- 236 12. J. Hadfield *et al.*, Nextstrain: real-time tracking of pathogen evolution. *Bioinformatics* **34**, 4121-  
237 4123 (2018).
- 238 13. C. Gao *et al.*, SARS-CoV-2 Spike Protein Interacts with Multiple Innate Immune Receptors. *bioRxiv*,  
239 2020.2007.2029.227462 (2020).
- 240 14. M. Sanda, L. Morrison, R. Goldman, N- and O-Glycosylation of the SARS-CoV-2 Spike Protein. *Anal  
241 Chem* **93**, 2003-2009 (2021).
- 242 15. X. Xie *et al.*, An Infectious cDNA Clone of SARS-CoV-2. *Cell Host Microbe* **27**, 841-848 e843 (2020).
- 243 16. X. Xie *et al.*, Engineering SARS-CoV-2 using a reverse genetic system. *Nature Protocols* **16**, 1761-  
244 1784 (2021).
- 245 17. T. P. Peacock *et al.*, The altered entry pathway and antigenic distance of the SARS-CoV-2 Omicron  
246 variant map to separate domains of spike protein. *bioRxiv*, 2021.2012.2031.474653 (2022).
- 247 18. B. Meng *et al.*, Altered TMPRSS2 usage by SARS-CoV-2 Omicron impacts infectivity and  
248 fusogenicity. *Nature* **603**, 706-714 (2022).
- 249 19. K. S. Phadke, N. B. A. Higdon, B. H. Bellaire, *In vitro* comparison of SARS-CoV-2  
250 variants. *bioRxiv*, 2023.2003.2011.532212 (2023).
- 251 20. H. Zhao *et al.*, SARS-CoV-2 Omicron variant shows less efficient replication and fusion activity  
252 when compared with Delta variant in TMPRSS2-expressed cells. *Emerging Microbes & Infections*  
253 **11**, 277-283 (2022).
- 254 21. C.-L. Hsieh *et al.*, Structure-based design of prefusion-stabilized SARS-CoV-2 spikes. *Science* **369**,  
255 1501-1505 (2020).
- 256 22. Z. Mustafa, H. Kalbacher, T. Burster, Occurrence of a novel cleavage site for cathepsin G adjacent  
257 to the polybasic sequence within the proteolytically sensitive activation loop of the SARS-CoV-2  
258 Omicron variant: The amino acid substitution N679K and P681H of the spike protein. *PLOS ONE*  
259 **17**, e0264723 (2022).

260 23. S. Yuan *et al.*, Pathogenicity, transmissibility, and fitness of SARS-CoV-2 Omicron in Syrian  
261 hamsters. *Science* **377**, 428-433 (2022).

262 24. C. P. McCormack *et al.*, Modelling the viral dynamics of the SARS-CoV-2 Delta and Omicron  
263 variants in different cell types. *bioRxiv*, 2023.2003.2015.529513 (2023).

264 25. K. P. Y. Hui *et al.*, SARS-CoV-2 Omicron variant replication in human bronchus and lung ex vivo.  
265 *Nature* **603**, 715-720 (2022).

266 26. A. M. Carabelli *et al.*, SARS-CoV-2 variant biology: immune escape, transmission and fitness.  
267 *Nature Reviews Microbiology* **21**, 162-177 (2023).

268 27. V. Papanikolaou *et al.*, From delta to Omicron: S1-RBD/S2 mutation/deletion equilibrium in SARS-  
269 CoV-2 defined variants. *Gene* **814**, 146134 (2022).

270 28. L. B. Shrestha, C. Foster, W. Rawlinson, N. Tedla, R. A. Bull, Evolution of the SARS-CoV-2 omicron  
271 variants BA.1 to BA.5: Implications for immune escape and transmission. *Reviews in Medical  
272 Virology* **32**, e2381 (2022).

273 29. D. Deming *et al.*, Vaccine Efficacy in Senescent Mice Challenged with Recombinant SARS-CoV  
274 Bearing Epidemic and Zoonotic Spike Variants. *PLOS Medicine* **3**, e525 (2006).

275 30. J. Harcourt *et al.*, Severe Acute Respiratory Syndrome Coronavirus 2 from Patient with  
276 Coronavirus Disease, United States. *Emerging infectious diseases* **26**, 1266-1273 (2020).

277 31. B. A. Johnson *et al.*, Nucleocapsid mutations in SARS-CoV-2 augment replication and  
278 pathogenesis. *PLOS Pathogens* **18**, e1010627 (2022).

279

280

281 **Acknowledgments**

282 Research was supported by grants from NIAID of the NIH to (R01-AI153602 and R21-AI145400  
283 to VDM; R24-AI120942 (WRCEVA) to SCW). ALR was supported by a UTMB Institute for Human  
284 Infection and Immunity grant and the Sealy and Smith Foundation. Research was also supported  
285 by STARs Award provided by the University of Texas System to VDM and Data Acquisition award  
286 provided by the Institute for Human Infections and Immunity at UTMB to MNV. Trainee funding  
287 provided by NIAID of the NIH to MNV (T32-AI060549).

288 Mass spectrometry experiments and analysis was provided by the Mass Spectrometry Facility at  
289 the University of Texas Medical Branch (<https://www.utmb.edu/MSF>). Figures were created with  
290 BioRender.com

291 **Competing Interest Statement**

292 VDM has filed a patent on the reverse genetic system and reporter SARS-CoV-2. MNV and VDM  
293 have filed a provisional patent on a stabilized SARS-CoV-2 spike protein. Other authors declare  
294 no competing interests.

295 **Author contributions**

296 Conceptualization: MNV, VDM

297 Formal analysis: MNV, VDM

298 Funding acquisition: MNV, ALR, SCW, VDM

299 Investigation: MNV, DRM, REA, KL, CS, JAP, LKE, AMM, YPA, WMM, ALM, JM, DHW, KP, ALR

300 Methodology: MNV, KSP, VDM

301 Project Administration: MNV, VDM

302 Supervision: MNV, SCW, DHW, KSP, VDM

303 Visualization: MNV, DHW, VDM

304 Writing – original draft: MNV, VDM

305 Writing – review and editing: MNV, REA, CS, DHW, VDM, SCW

306 **Figure Legends**

307 **Figure 1. The combination of Omicron mutations H655Y, N679K, and P681H increases viral**  
308 **replication and spike processing.**

309 **(A)** Comparison of CTS1 region near the S1/S2 cleavage site between SARS-CoV-2 variants.

310 **(B)** Structure of loop containing the S1/S2 cleavage site on SARS-CoV-2 spike protein. The  
311 residues that are mutated in Omicron are shown: H655 (magenta), N679 (green), and P681  
312 (blue). The furin cleavage site RRAR (cyan) and QTQT motif (red) are also shown.

313 **(C)** Schematic of WT and YKH SARS-CoV-2 mutant genomes.

314 **(D)** WT and YKH SARS-CoV-2 plaques on Vero E6 cells at 2 dpi.

315 **(E)** Viral titer from WT and YKH virus stocks representing the highest yield generated from  
316 TMPRSS2-expressing Vero E6 cells.

317 **(F-G)** Replication kinetics of WT and YKH in Vero E6 **(F)** and Calu-3 2B4 **(G)** cells. Cells were  
318 infected at an MOI of 0.01 infectious units/cell (n=3). Data are mean  $\pm$  s.d. Statistical analysis  
319 measured by two-tailed Student's t-test.

320 **(H)** Purified WT, YKH, Delta isolate (B.1.617.2), and Omicron (BA.1) virions from Vero E6  
321 supernatant were probed with  $\alpha$ -Spike and  $\alpha$ -Nucleocapsid (N) antibodies in Western blots. Full-  
322 length spike (FL), S1/S2 cleavage product, and S2' cleavage product are indicated.

323 **(I)** Densitometry of FL and S1/S2 cleavage product was performed, and quantification of FL and  
324 S1/S2 cleavage product percentage of total spike is shown. Quantification was normalized to N  
325 for viral protein loading control. WT (black), YKH (blue), Delta isolate (purple), Omicron (orange).  
326 Results are representative of two experiments.

327 **Figure 2. N679K attenuates SARS-CoV-2 replication and disease.**

328 **(A)** Structural modeling of O-linked glycosylation of threonine 678 (yellow) of QTQTN motif (red)  
329 and the residues mutated in Omicron – H655 (magenta), N679 (green), and P681 (blue) – with  
330 N679 adjacent to the glycosylation. The furin cleavage site RRAR is also shown (cyan).

331 **(B)** Schematic of WT and N679K SARS-CoV-2 genomes.

332 **(C)** WT and N679K SARS-CoV-2 plaques on Vero E6 cells at 2 (left) and 3 dpi (right). Average  
333 plaque sizes noted below.

334 **(D)** Viral titer from WT and N679K virus stocks with the highest yield generated from TMPRSS2-  
335 expressing Vero E6 cells.

336 **(E-F)** Replication kinetics of WT and N679K in Vero E6 **(E)** and Calu-3 2B4 **(F)** cells. Cells were  
337 infected at an MOI of 0.01 infectious units/cell (n=3). Data are mean  $\pm$  s.d. Statistical analysis  
338 performed using two-tailed Student's t-test.

339 **(G)** Schematic of experimental design for golden Syrian hamster infection with WT (black) or  
340 N679K (green) SARS-CoV-2. Three- to four-week-old male hamsters were infected with  $10^5$  pfu  
341 and monitored for weight loss over 7 days. At 2, 4, and 7 dpi, nasal washes and lungs were  
342 collected for viral titer, and lung was collected for histopathology.

343 **(H)** Weight loss of hamsters infected with WT (black) or N679K (green) SARS-CoV-2 over 7 days.  
344 Data are mean  $\pm$  s.e.m. Statistical analysis measured by two-tailed Student's t-test.

345 **(I-J)** Viral titers of lungs **(I)** and nasal washes **(J)** collected at 2 and 4 dpi from hamsters infected  
346 with WT (black) or N679K (green) SARS-CoV-2. Data are mean  $\pm$  s.d. Statistical analysis  
347 measured by two-tailed Student's t-test.

348 **Figure 3. N679K results in decreased spike expression on virions and in infected cells.**

349 **(A)** Purified WT, N679K, and Omicron (BA.1) virions from Vero E6 supernatants were probed with  
350  $\alpha$ -Spike and  $\alpha$ -Nucleocapsid (N) antibodies in Western blots. Full-length spike (FL), S1/S2  
351 cleavage product, and S2' cleavage product are indicated.

352 **(B)** Densitometry of spike processing from purified virions applied to Western blots in **(A)** was  
353 performed, and quantification of FL and S1/S2 cleavage product percentage of total spike is  
354 shown. Quantification was normalized to N as viral protein loading control. WT (black), N679K  
355 (green), Omicron (orange). Results are representative of two experiments.

356 **(C)** Densitometry of spike expression from purified virion Western blots in **(A)** was performed, and  
357 quantification of total spike protein to nucleocapsid ratio is shown. Spike/N ratio is relative to WT.  
358 WT (black), N679K (green), Omicron (orange). Results are representative of two experiments.

359 **(D)** Vero E6 cells were infected with WT, N679K, or Omicron at an MOI of 0.01 infectious  
360 units/cell. Cell lysate was collected at 24 hpi and probed with  $\alpha$ -Spike and  $\alpha$ -Nucleocapsid (N)  
361 antibodies in Western blots. Full-length spike (FL), S1/S2 cleavage product, and S2' cleavage  
362 product are indicated.

363 **(E)** Densitometry of spike expression from infected cell lysate Western blots in **(D)** was performed,  
364 and quantification of total spike protein to nucleocapsid ratio is shown. Spike/N ratio is relative to  
365 WT. WT (black), N679K (green), Omicron (orange). Results are representative of three biological  
366 replicates.

367 **(F)** Vero E6 cells were transfected with Spike HexaPro WT and N679K and cell lysate was  
368 collected at 8, 24, and 48 hpt. Lysates were probed with  $\alpha$ -Spike and  $\alpha$ -GAPDH antibodies in  
369 Western blots.

370 (G) Densitometry of spike expression from transfected cell lysates by Western blot in (G) was  
371 performed, and quantification of relative total spike protein is shown. Spike protein levels were  
372 normalized to GAPDH and are relative to WT. WT (black), N679K (green). Results are  
373 representative of three biological replicates.

374 **Methods**

375 **Cell Culture**

376 Vero E6 cells were grown in high glucose DMEM (Gibco #11965092) with 10% fetal bovine serum  
377 and 1x antibiotic-antimycotic. TMPRSS2-expressing Vero E6 cells were grown in low glucose  
378 DMEM (Gibco #11885084) with sodium pyruvate, 10% FBS, and 1 mg/mL Geneticin<sup>TM</sup> (Invitrogen  
379 #10131027). Calu-3 2B4 cells were grown in high glucose DMEM (Gibco #11965092) with 10%  
380 defined fetal bovine serum, 1 mM sodium pyruvate, and 1x antibiotic-antimycotic.

381 **Viruses**

382 The SARS-CoV-2 infectious clones were based on the USA-WA1/2020 sequence provided by  
383 the World Reference Center of Emerging Viruses and Arboviruses and the USA Centers for  
384 Disease Control and Prevention (30). Mutant viruses (YKH and N679K) were generated with  
385 restriction enzyme-based cloning using gBlocks encoding the mutations (Integrated DNA  
386 Technologies) and our reverse genetics system as previously described (15, 16). Virus stock was  
387 generated in TMPRSS2-expressing Vero E6 cells to prevent mutations from occurring at the  
388 FCS. Viral RNA was extracted from virus stock and cDNA was generated to verify mutations by  
389 Sanger sequencing.

390 Delta isolate (B.1.617.2) was obtained from the World Reference Center of Emerging Viruses and  
391 Arboviruses. Infectious clone of Omicron (BA.1) was obtained from Dr. Pei Yong Shi and Dr.  
392 Xuping Xie.

393 ***In vitro* Infection**

394 Vira infections in Vero E6 and Calu-3 2B4 were carried out as previously described (8). Briefly,  
395 growth media was removed, and cells were infected with WT or mutant SARS-CoV-2 at an MOI  
396 of 0.01 for 45 min at 37°C with 5% CO<sub>2</sub>. After absorption, cells were washed three times with PBS  
397 and fresh complete growth media was added. Three or more biological replicates were collected  
398 at each time point and each experiment was performed at least twice. Samples were titrated with  
399 plaque assay or focus forming assays.

400 **Plaque Assay**

401 Vero E6 cells were seeded in 6-well plates and grown to 80-100% confluence in complete growth  
402 media. Ten-fold serial dilutions in PBS were performed on virus samples. Growth media was  
403 removed from cells and 200  $\mu$ l of inoculum was added to monolayers. Cells were incubated for  
404 45 min at 37°C with 5% CO<sub>2</sub>. After absorption, 0.8% agarose overlay was added, and cells were  
405 incubated at 37°C with 5% CO<sub>2</sub> for 2 days. Plaques were visualized with neutral red stain. Average  
406 plaque size was determined using ImageJ.

407 **Focus Forming Assay**

408 Focus forming assays (FFAs) were performed as previously described (31). Briefly, Vero E6 cells  
409 were seeded in 96-well plates to be 100% confluent. Samples were 10-fold serially diluted in  
410 serum-free media and 20  $\mu$ l was to infect cells. Cells were incubated for 45 min at 37°C with 5%  
411 CO<sub>2</sub> before 100  $\mu$ l of 0.85% methylcellulose overlay was added. Cells were incubated for 24 h 45  
412 min at 37°C with 5% CO<sub>2</sub>. After incubation, overlay was removed, and cells were washed three  
413 times with PBS before fixed and virus inactivated by 10% formalin for 30 min at room temperature.  
414 Cells were then permeabilized and blocked with 0.1% saponin/0.1% BSA in PBS before incubated  
415 with  $\alpha$ -SARS-CoV-2 Nucleocapsid primary antibody (Cell Signaling Technology) at 1:1000 in  
416 permeabilization/blocking buffer overnight at 4°C. Cells are then washed three times with PBS  
417 before incubated with Alexa Fluor<sup>TM</sup> 555-conjugated  $\alpha$ -mouse secondary antibody (Invitrogen  
418 #A28180) at 1:2000 in permeabilization/blocking buffer for 1 h at room temperature. Cells were  
419 washed three times with PBS. Fluorescent foci images were captured using a Cytation 7 cell  
420 imaging multi-mode reader (BioTek), and foci were counted manually.

421 **Hamster Infection**

422 Three- to four-week-old male golden Syrian hamsters (HsdHan:AURA strain) were purchased  
423 from Envigo. All studies were conducted under a protocol approved by the UTMB Institutional  
424 Animal Care and Use Committee and complied with USDA guidelines in a laboratory accredited  
425 by the Association for Assessment and Accreditation of Laboratory Animal Care. Procedures

426 involving infectious SARS-CoV-2 were performed in the Galveston National Laboratory ABSL3  
427 facility. Hamsters were intranasally infected with  $10^5$  pfu of WT or N679K SARS-CoV-2 in 100  $\mu$ l.  
428 Infected hamsters were weighed and monitored for illness over 7 days. Hamsters were  
429 anesthetized with isoflurane and nasal washes were collected with 400  $\mu$ l of PBS on endpoint  
430 days (2, 4, and 7 dpi). Hamsters were euthanized by CO<sub>2</sub> for organ collection. Nasal wash and  
431 lung were collected to measure viral titer and RNA. Left lungs were collected for histopathology.

#### 432 **Virion Purification**

433 Vero E6 cells were grown in T175 flasks to be 100% confluent at time of infection. Cells were  
434 infected with 50  $\mu$ l of virus stock in PBS for 45 min at 37°C with 5% CO<sub>2</sub>, and growth media with  
435 5% FBS was added after absorption. Supernatant was harvested at 24 hpi and clarified by low-  
436 speed centrifugation. Virions were purified from supernatant by ultracentrifugation through a 20%  
437 sucrose cushion at 26,000 rpm for 3 hrs using a Beckman SW28 rotor. Pellets were resuspended  
438 with 2x Laemmli buffer to obtain protein samples for Western blot.

#### 439 **Western Blot**

440 Protein levels were determined by SDS-PAGE followed by western blot analysis as previously  
441 described (8). In brief, sucrose-purified SARS-CoV-2 virions were inactivated by resuspending in  
442 2x Laemmli buffer and boiling. SDS-PAGE gels were run with equal volumes of samples on Mini-  
443 PROTEAN TGX gels (Bio-Rad #4561094) followed by transfer onto PVDF membrane.  
444 Membranes were incubated with  $\alpha$ -SARS-CoV S primary antibody (Novus Biologicals #NB100-  
445 56578) at 1:1000 dilution in 5% BSA in TBST to measure spike protein processing and  
446 expression. For loading control,  $\alpha$ -SARS Nucleocapsid primary antibody (Novus Biologicals  
447 #NB100-56576) at 1:1000 in 5% BSA in TBST was used for viral loading control and  $\alpha$ -GAPDH  
448 primary antibody (Invitrogen #AM4300) at 1:1000 in 5% BSA in TBST for cellular loading control.  
449 Primary antibody incubation was followed by HRP-conjugated  $\alpha$ -rabbit secondary antibody (Cell  
450 Signaling Technology #7074) or HRP-conjugated  $\alpha$ -mouse secondary antibody (Cell Signaling  
451 Technology #7076) at 1:3000 in 5% milk in TBST. Chemiluminescence signal was developed

452 using Clarity Western ECL substrate (Bio-Rad #1705060) or Clarity Max Western ECL substrate  
453 (Bio-Rad #1705062) and imaged with a ChemiDoc MP System (Bio-Rad). Densitometry analysis  
454 was performed using ImageLab 6.0.1 (Bio-Rad).

#### 455 **Spike HexaPro Cloning and Transfection**

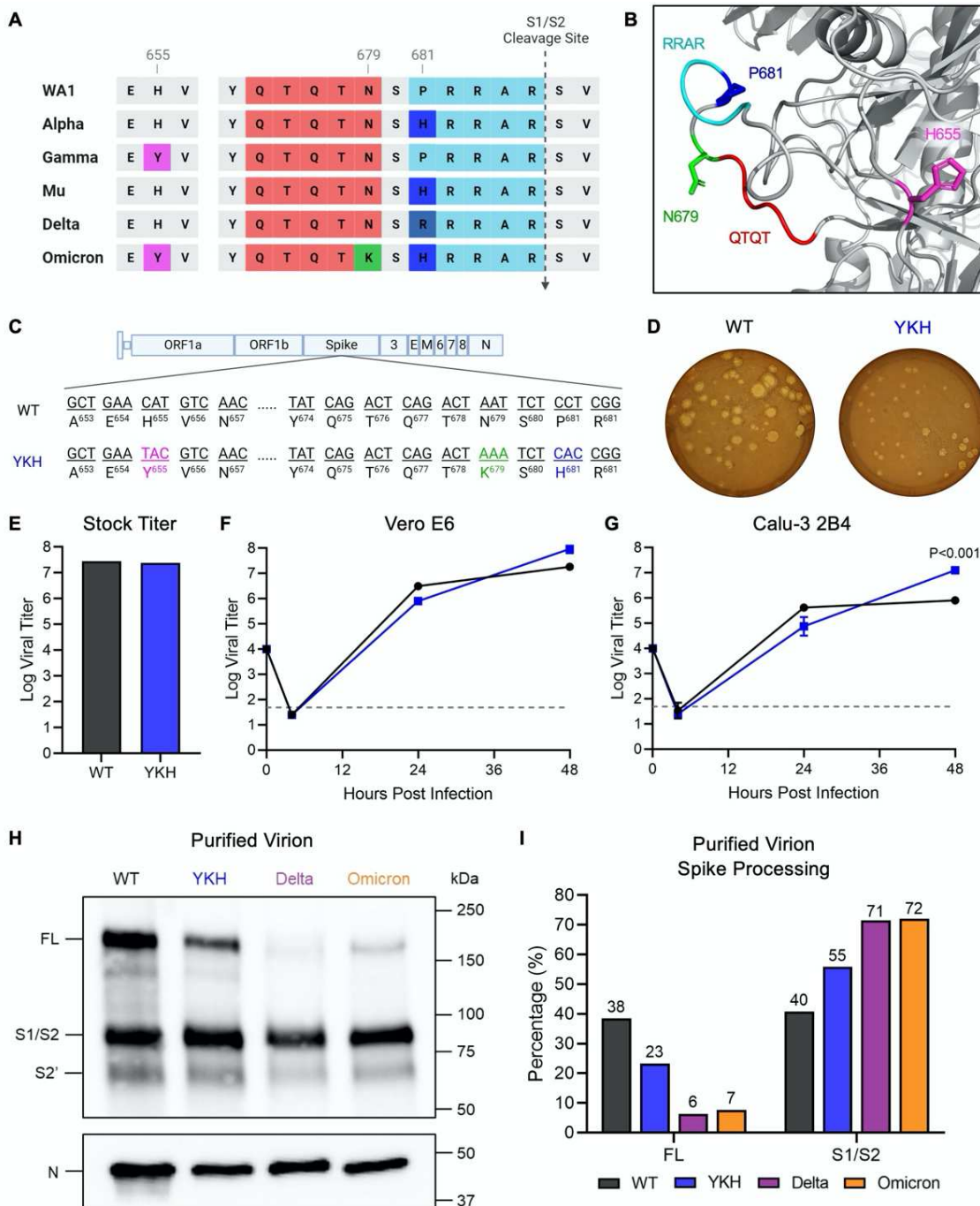
456 SARS-CoV-2 S HexaPro was a gift from Jason McLellan (Addgene plasmid #154754) (21). The  
457 N679K mutation was cloned into spike HexaPro using a gBlock encoding the mutation (Integrated  
458 DNA Technologies) and restriction enzyme-based cloning. Sequences were verified by Sanger  
459 sequencing.

460 Vero E6 cells were grown in 24-well plates to be 100% confluent at time of transfection. Cells  
461 were transfected with spike HexaPro WT or N679K plasmid and Lipofectamine 2000 following  
462 manufacturer's instructions (Invitrogen). Briefly, 100 ng of spike HexaPro plasmid and 1.5  $\mu$ l of  
463 Lipofectamine 2000 were separately diluted in 50  $\mu$ l Opti-MEM (Gibco #31985070) before mixing  
464 together. After 20 min of room temperature incubation, 100  $\mu$ l of the transfection mixture was  
465 added to cells, and cells were incubated at 37°C with 5% CO<sub>2</sub>. Cell lysate was harvested with 2x  
466 Laemmli buffer at 24 and 48 hours post transfection to be analyzed by Western blot.

#### 467 **Structural Modeling**

468 Structural models previously generated were used as a base to visualize residues mutated in  
469 Omicron (8). Briefly, structural models were generated using SWISS-Model to generate homology  
470 models for WT and glycosylated SARS-CoV-2 spike protein on the basis of the SARS-CoV-1  
471 trimer structure (Protein Data Bank code 6ACD). Homology models were visualized and  
472 manipulated in PyMOL (version 2.5.4) to visualize Omicron mutations.

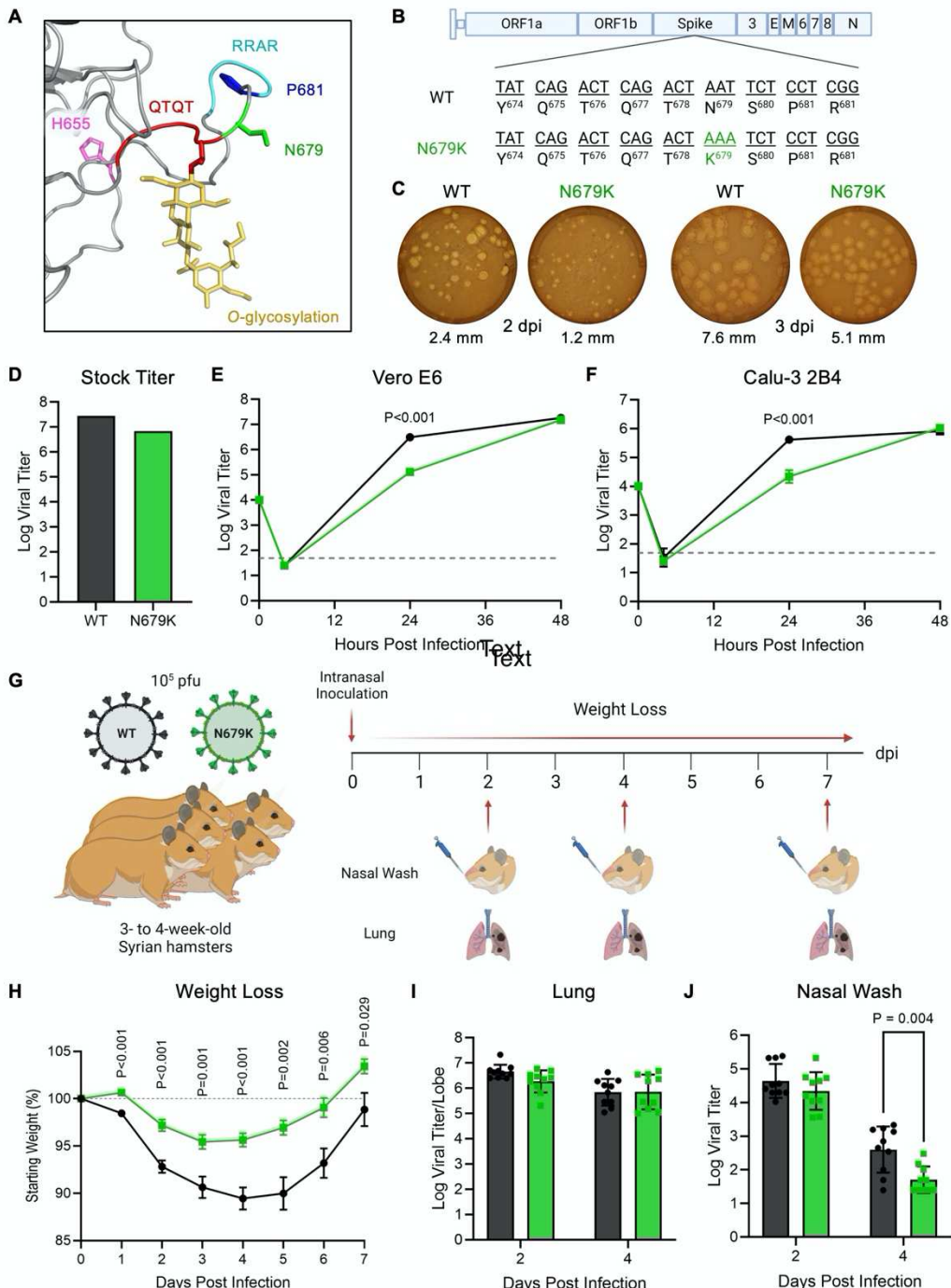
473



474

475 **Figure 1. The combination of Omicron mutations H655Y, N679K, and P681H increases viral replication and spike processing.**  
476 (A) Comparison of CTS1 region near the S1/S2 cleavage site between SARS-CoV-2 variants. (B) Structure of loop containing the  
477 S1/S2 cleavage site on SARS-CoV-2 spike protein. The residues that are mutated in Omicron are shown – H655 (magenta), N679  
478 (green), and P681 (blue). The furin cleavage site RRAR (cyan) and QTQT motif (red) are also shown. (C) Schematic of WT and YKH  
479 SARS-CoV-2 mutant genomes. (D) WT and YKH SARS-CoV-2 plaques on Vero E6 cells at 2 dpi. (E) Viral titer from WT and YKH in Vero  
480 E6 (F) and Calu-3 2B4 (G) cells. Cells were infected at an MOI of 0.01 (n=3). Data are mean  $\pm$  s.d. Statistical analysis measured by  
481 two-tailed Student's t-test. (H) Purified WT, YKH, Delta isolate (B.1.617.2), and Omicron (BA.1) virions from Vero E6 supernatant were  
482 probed with  $\alpha$ -Spike and  $\alpha$ -Nucleocapsid (N) antibodies in Western blots. Full-length spike (FL), S1/S2 cleavage product, and S2'  
483 cleavage product are indicated. (I) Densitometry of FL and S1/S2 cleavage product was performed, and quantification of FL and S1/S2  
484 cleavage product percentage of total spike is shown. Quantification was normalized to N for viral protein loading control. WT (black),  
485 YKH (blue), Delta isolate (purple), Omicron (orange). Results are representative of two experiments.

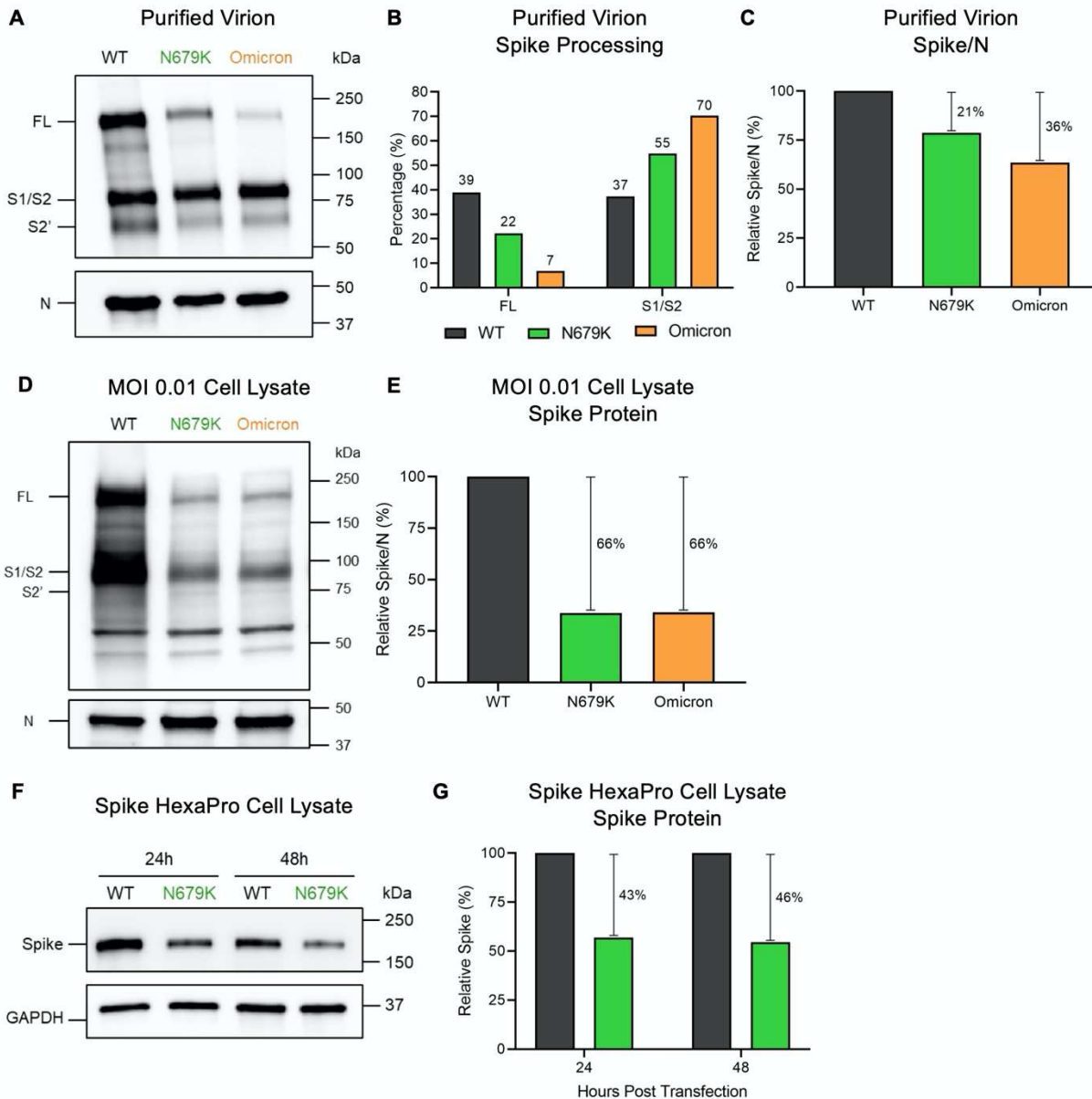
486



**Figure 2. N679K attenuates SARS-CoV-2 replication and disease when isolated.**  
 (A) Structural modeling of O-linked glycosylation of threonine 678 (yellow) of QTQTN motif (red) and the residues mutated in Omicron – H655 (magenta), N679 (green), and P681 (blue) – with N679 adjacent to the glycosylation. The furin cleavage site RRAR is also shown (cyan). (B) Schematic of WT and N679K SARS-CoV-2 genomes. (C) WT and N679K SARS-CoV-2 plaques on Vero E6 cells at 2 dpi (left) and 3 dpi (right). Average plaque size noted below. (D) Viral titer from WT and N679K virus stock with the highest yield generated from TMPRSS2-expressing Vero E6 cells. (E-F) Growth kinetics of WT and N679K in Vero E6 (E) and Calu-3 2B4 (F) cells. Cells were infected at an MOI of 0.01 (n=3). Data are mean  $\pm$  s.d. Statistical analysis measured by two-tailed Student's t-test. (G) Schematic of experiment design for golden Syrian hamster infection with WT (black) or N679K (green) SARS-CoV-2. Three- to four-week-old male hamsters were infected with  $10^5$  pfu and monitored for weight loss over 7 days. At 2, 4, and 7 dpi, nasal wash and lung was collected for viral titer, and lung was collected for histopathology. (H) Weight loss of hamsters infected with WT (black) or N679K (green) SARS-CoV-2 over 7 days. Data are mean  $\pm$  s.e.m. Statistical analysis measured by two-tailed Student's t-test. (I-J) Viral titer of lung (I) and nasal wash (J) collected at 2 and 4 dpi from hamsters infected with WT (black) or N679K (green) SARS-CoV-2. Data are mean  $\pm$  s.d. Statistical analysis measured by two-tailed Student's t-test.

487  
488

489  
490  
491  
492  
493  
494  
495  
496  
497  
498  
499  
500



501  
502 **Figure 3. N679K results in decreased spike expression on virions and in cell lysate.** (A) Purified WT, N679K, and Omicron  
503 (BA.1) virions from Vero E6 supernatant were probed with  $\alpha$ -Spike and  $\alpha$ -Nucleocapsid (N) antibodies in Western blots. Full-length  
504 spike (FL), S1/S2 cleavage product, and S2' cleavage product are indicated. (B) Densitometry of spike processing from purified virion  
505 Western blot in (A) was performed, and quantification of FL and S1/S2 cleavage product percentage of total spike is shown.  
506 Quantification was normalized to N as viral protein loading control. WT (black), N679K (green), Omicron (orange). Results are  
507 representative of two experiments. (C) Densitometry of spike expression from purified virion Western blot in (A) was performed, and  
508 quantification of total spike protein to nucleocapsid ratio is shown. Spike/N ratio is relative to WT. WT (black), N679K (green), Omicron  
509 (orange). Results are representative of two experiments. (D) Vero E6 cells were infected with WT, N679K, or Omicron at an MOI of  
510 0.01. Cell lysate was collected at 24 hpi and probed with  $\alpha$ -Spike and  $\alpha$ -Nucleocapsid (N) antibodies in Western blots. Full-length  
511 spike (FL), S1/S2 cleavage product, and S2' cleavage product are indicated. (E) Densitometry of spike expression from infected cell  
512 lysate Western blot in (D) was performed, and quantification of total spike protein to nucleocapsid ratio is shown. Spike/N ratio is  
513 relative to WT. WT (black), N679K (green), Omicron (orange). Results are representative of three biological replicates. (F) Vero E6  
514 cells were transfected with Spike HexaPro WT and N679K and cell lysate was collected at 8, 24, and 48 hpt. Lysates were probed  
515 with  $\alpha$ -Spike and  $\alpha$ -GAPDH antibodies in Western blots. (G) Densitometry of spike expression from transfected cell lysate Western  
516 blot in (F) was performed, and quantification of relative total spike protein is shown. Spike protein levels were normalized to GAPDH  
517 and are relative to WT. WT (black), N679K (green). Results are representative of three biological replicates.